Published in final edited form as:
J Am Chem Soc. 2010 May 19; 132(19): 6679–6685. doi:10.1021/ja909456f.

Shape-enhanced Photocatalytic Activity of Single-crystalline Anatase TiO_2 (101) Nanobelts

Nianqiang Wu[1,*], **Jin Wang**[1], **De Nyago Tafen**[2], **Hong Wang**[2], **Jian-Guo Zheng**[3], **James P. Lewis**[2], **Xiaogang Liu**[4], **Stephen S. Leonard**[5], and **Ayyakkannu Manivannan**[6]

[1]Department of Mechanical and Aerospace Engineering, WVNano Initiative, West Virginia University, Morgantown, WV 26506-6106, USA

[2]Department of Physics, West Virginia University, Morgantown, WV 26506, USA

[3]Materials Characterization Center (MC2), LEXI, California Institute for Telecommunication and Information Technology, University of California, Irvine, CA 92697, USA

[4]Department of Chemistry, National University of Singapore, Singapore 117543

[5]National Institute for Occupational Safety and Health, Morgantown, WV 26505, USA

[6]National Energy Technology Laboratory, U.S. Department of Energy, Morgantown, WV 26507, USA

Abstract

Particle size is generally considered to be the primary factor in design of nanocrystal photocatalyst, because the reduction of particle size increases the number of active sites. However, the benefit from the size reduction can be canceled by a higher electron-hole recombination rate due to the confined space in sphere-shaped nanoparticles. Here we report a mechanistic study on a novel nanobelt structure that overcomes the drawback of sphere-shaped nanoparticles. Single-crystalline anatase TiO_2 nanobelts with two dominant surfaces of (101) facet exhibit enhanced photocatalytic activity than the nanosphere counterparts with an identical crystal phase and similar specific surface area. The *ab initio* density functional theory (DFT) calculations show that the exposed (101) facet of the nanobelts yields an enhanced reactivity with molecular O_2, facilitating the generation of superoxide radical. Moreover, the nanobelts exhibit a lower electron-hole recombination rate than the nanospheres due to the following three reasons: (i) greater charge mobility in the nanobelts, which is enabled along the longitudinal dimension of the crystals; (ii) fewer localized states near the band edges and in the bandgap due to less unpassivated surface states in the nanobelts; and (iii) enhanced charge separation due to trapping of photogenerated electrons by chemisorbed molecular O_2 on the (101) facet. Our results suggest that the photocatalysis efficiency of nanocrystals can be significantly improved by tailoring the shape and the surface structure of nanocrystals, which provides a new concept for rational design and development of high-performance photocatalysts.

Keywords

titanium dioxide; photocatalysis; nanobelt; nanowire; titania; photocatalyst

[*]Corresponding author: Tel: +1(304)-293-3326, Fax: +1-(304)-293-6689, nick.wu@mail.wvu.edu.

Supporting Information Available: XRD patterns of the TiO_2 nanobelts nanospheres are presented in Figure S1. The SEM image of the TiO_2 nanospheres is shown in Figure S2. Degradation of methyl orange in an aqueous solution saturated with oxygen, nitrogen and air is shown in Figure S3. Photoluminescence spectra of the TiO_2 nanobelts and the nanospheres are presented in Figure S4. Method for determining the facet of two major exposed surfaces of the nanobelts is also shown. This material is available free of charge via the Internet at http://pubs.acs.org.

1. Introduction

Titanium oxide photocatalysts are of great importance due to increasing applications in hydrogen generation, solar energy utilization, environmental remediation and biomedical applications.[1–4] Photocatalysis of TiO_2 generally involves four processes:[1–4] (i) generation of electrons and holes by photoexcitation; (ii) migration of the photogenerated charge carriers to the surface; (iii) subsequent reduction/oxidization of the adsorbed reactants directly by electrons/holes or by reactive oxygen species (ROS); and (iv) recombination of the photogenerated electron-hole pairs. Desired photocatalysts are expected to promote Process (i), (ii) and (iii) in the meanwhile to suppress Process (iv). Smaller particles are generally preferred to be used as photocatalysts due to higher specific surface area, leading to more surface reactive sites. However, for commonly used sphere-shaped nanoparticles (called nanospheres), the benefit from the size reduction would be canceled by a higher electron-hole recombination rate,[5] because the photogenerated electrons and holes may not be efficiently separated from each other in the confined space.6 Recent studies have shown that the geometry of nanoparticles has significant effect on the photoelectrolysis activity7. TiO_2 nanotubes act as electron highway that exhibit superior electron transport capability in dye-sensitized solar cells8.[9]. We postulate that one dimensional (1-D) single-crystalline nanostructures such as nanobelts, nanowires and nanotubes would retain high specific surface area but have a lower charge carrier recombination rate as compared to nanospheres. This postulation has built on a hypothesis that charge carriers are less localized in 1-D nanostructured single crystals where the photogenerated electrons and holes are free to transport throughout the whole length dimension of the crystal due to high degree of crystallinity and the absence of grain boundaries in the 1-D nanostructured single crystal. It is well known that grain boundaries and other defects act as the recombination sites for electrons and holes.[10]

In addition, the photocatalytic activity of TiO_2 crystals is heavily dependent upon the surface structure (surface atomic arrangement and coordination)[11–14] especially when the particle size is reduced to the nanometer length scale, leading to large specific surface area. For example, the rutile (100) and (110) facets exhibit lower photoreduction rates toward conversion of Ag^+ to metallic Ag than the (101), (111), and (001) facets.[11] Potentially, photoreduction and photooxidation are predominant on different crystal facets. For instance, the rutile {011} facets provide the metal oxidation sites while the {110} facets offer the metal reduction sites. 14 Recent investigations have revealed that the anatase TiO_2 nanocrystals with well-faceted {101} surfaces exhibit enhanced photocatalytic activity.[9,15] These studies have shown that the photocatalytic activity of TiO_2 can be tailored by controlling the exposed crystal facets of particles although the underlying mechanism is not well understood. As of now, the information on the crystal facet effect on photocatalytic activity is limited, because TiO_2 nanocrystals with specific well-faceted surfaces are difficult to obtain. The reports on TiO_2 available in this research area are mainly gained from rutile single crystals,[12] because anatase TiO_2 single crystals with controlled specific well-faceted surfaces are rare in the literature.[16] So far, thin films and bulk TiO_2 single crystals are the major sources for studying the correlation of specific crystal facets with catalysis and the related surface phenomena. Thin films and bulk single crystals provide model systems for fundamental studies but cannot be applied to practical use due to their limited specific surface area.

Based on the above discussions, we have designed a unique shaped photocatalyst: single-crystalline anatase TiO_2 (101) nanobelt with the longitudinal dimension on the micron scale (or even longer) and the lateral dimension on the nanoscale. Here we present 60–400 nm wide, ~10 nm thick and up to 25 μm long nanobelts as an example. Reducing the lateral dimension down to the nanometer length scale offers high specific surface area while keeping the longitudinal dimension of single crystal at the large scale to minimize the electron-hole

recombination rate. The one-dimensionality provides a transport channel and sufficient space for charge separation. Moreover, the unique shape of our developed nanobelts provides the well-defined anatase (101) facet for two dominantly exposed surfaces. Such anisotropic surface facets could render it high photo-reactivity toward certain chemical species. Therefore, such nanobelts are expected to offer an enhanced photocatalytic activity than sphere-shaped particles with a diameter on the same scale as the lateral dimension of the nanobelts. To the best of our knowledge, we report here for the first time a systematic study on the effects of the shape and the surface structure on the photocatalytic activity of TiO_2 nanobelts. In particular, we present a comparative study of the photocatalytic activities of nanobelts and nanospheres in order to clarify the underlying mechanism of the enhanced photocatalysis performance of the anatase TiO_2 (101) nanobelt photocatalysts.

2. Experimental Methods

Nanobelt synthesis

The TiO_2 nanobelts were prepared by hydrothermal treatment. Titanium dioxide powder (Alfa Aesar) was added into a 10 M NaOH aqueous solution in a Teflon-lined stainless steel autoclave. The autoclave was sealed and subsequently heated at 200 °C for 24 hours. After hydrothermal processing, white fluffy product was washed with copious deionized water and 0.1 M hydrochloric acid until the pH of the washing solution is reduced to ≤7. The as-washed samples were then calcinated at 700 °C for 30 min at a ramp rate of 1 °C/min. For comparison tests, the TiO_2 nanospheres were purchased directly from Alfa Aesar without further purification.

Material characterization

The UV-Vis absorption spectra were measured under the diffuse reflection mode using a Shimadzu 2550 UV-Visible spectrometer equipped with an integrating sphere (UV2401/2, Shimadzu). The photoluminescence (PL) spectra were acquired at room temperature with a Hitachi F-7000 fluorescence spectrophotometer under the ultraviolet excitation of 250 nm. The specific surface area of the particles was measured by Brunauer-Emmett-Teller (BET) method (Accelerated Surface Area and Porosity System 2020, Micromeritics). The particle morphology was observed with a Hitachi S4700 field-emission scanning electron microscope (SEM). The crystal structure of the TiO_2 particles was characterized by X-ray diffraction (XRD, X'Pert Pro PW3040-Pro, Panalytical Inc.) with Cu Kα radiation, transmission electron microscope (TEM), high resolution transmission electron microscopy (HRTEM) and selected area electron diffraction (SAED) (a 200 kV FEI/Philips CM20 TEM apparatus). For TEM sample preparation, the powders were suspended in ethanol, and then a drop of this suspension was deposited onto a holey carbon film supported by a copper grid. The TEM specimen was dried in air prior to the TEM examination.

Photocatalysis experiments

The photocatalysis experiments were carried out in a commercial photoreactor (LUZ-4V, Luzchem) equipped with the 148 W UVA lamp (Centered at 350 nm, LZC-UVA, Luzchem). A total of 10 mg TiO_2 catalysts were added to 10 ml solution of 20 mg/L methyl orange in a 10 ml polyethylene tube. Before irradiation, the suspensions were sonicated in the dark for 5 minutes. During irradiation, the tubes were placed onto the carousel inside the photoreactor to ensure the even exposure of each tube to the ultraviolet A (UVA) light. At the different time intervals of irradiation, the tubes were unloaded and then centrifuged at 10,000 rpm for 1.5 hours to separate the supernate and the catalysts. The supernates were collected and analyzed by recording the characteristic absorption peak of methyl orange (464 nm) using a UV-Vis spectrometer. According to the calibration plot of the UV absorbance as a function of the

remaining methyl orange concentration, the efficiency of the methyl orange decomposition was calculated.

Radical measurement

Following the approach developed by Uchino *et al*,[17] the $OH^{\bullet}$ radicals generated by the TiO_2 particles under ultraviolet (UV) irradiation were quantified with an X-band electron spin resonance (ESR) spectroscopy/spin-trapping technique. A suspension of TiO_2 particles (100 mg/L) was mixed with a $OH^{\bullet}$ radical spin-trapping agent- 5,5-dimethyl-1-pyrroline-N-oxide (DMPO, 100 mM) in the aqueous solution. This solution was kept in the dark for 30 minutes and then irradiated with the UVA lamps at an emission maximum at 350 nm for 5 minutes. The ESR spectra were subsequently acquired with an ESR spectrometer at an ambient temperature.

DFT calculations

An *ab initio* tight-binding method, called *FIREBALL*, which is based on density functional theory with nonlocal pseudopotentials within the local density approximation (LDA),[18] was used to simulate the electronic structure of the anatase TiO_2 nanobelts and nanospheres. The confined atomic-like orbitals were used as a basis set for determination of the occupied eigenvalues and eigenvectors of the one-electron Hamiltonian. The calculation was undertaken entirely in real space, which provided substantial computational efficiency. Hamiltonian and overlap matrix elements are precalculated on a numerical grid and the specific values needed for a particular instantaneous conformation are extracted from the tabulated values via interpolation. Naturally, the integral tables need to be generated only once, for a given set of atomic species, rather than performing quadratures "on the fly" during a molecular dynamics (MD) run. In the calculations, a minimal basis set for O and Ti was chosen with the addition of an excited *p*-state for polarization to the Ti ground-state configuration. This method has been successfully used for obtaining geometries and electronic properties of bulk TiO_2 material and TiO_2 nanostructures.[19,20] For the simulations reported here, the atomic structure of the nanobelts and nanospheres were carved out from anatase structure. For each nanostructure, the stoichiometry was preserved and no saturation of dangling bonds or charge embedding was applied. The initial geometries were fully relaxed to the nearest local minimum structure.

Since the transport mobility of the charge carriers in the anatase TiO_2 lattice is linearly related to conductivity, one can estimate the conductivity. It was reported21,[22] that the Kubo-Greenwood formula (KGF) built the natural approximate connection between the conductivity and the electronic states (localized states) and energies. Hence the Kubo formalism in conjunction with *ab inito* methods in FIREBALL was used to estimate the dc conductivity in the TiO_2 nanobelts and the nanospheres. The dc conductivity was computed from trajectory averaged quantities using the formulae developed by Abtew *et al*.[23] The well relaxed models of TiO_2 nanobelts and nanospheres were used in the present work. The models were prepared at room temperature (T=300K) for a total time of 15.0 ps. Once the models were well equilibrated, a constant temperature molecular dynamic (MD) simulation for 2000 steps (with the time step of 1.50 fs) was performed where data were collected after every 10 steps to obtain the average dc conductivity. During the calculation, the MD simulations were carried out in the NVT ensemble (i.e., the number of particles N, the volume V and the temperature T of the system are kept constant).

3. Results and Discussions

The BET adsorption analysis showed that the specific surface areas of the nanobelts and the nanospheres were 20.83 m^2/g and 57.70 m^2/g, respectively. Both the as-synthesized titania nanobelts and the commercial titania nanospheres exhibited the monolithic anatase phase, as

confirmed by the XRD patterns (Figure S1 in Supporting Information). The morphology of the nanospheres is revealed in Figure S2. The nanospheres are around 150 nm in diameter. Figure 1(a) shows the SEM image of the nanobelts. The nanobelts are 60–400 nm wide and ~10 nm thick. The length of the nanobelts varies from several microns to 30 μm. Figure 1(b) shows a bright-field TEM image taken from a single nanobelt that is about 180 nm wide and about 10 nm thick as determined from the TEM images observed from different directions. Electron diffraction data indicate that the nanobelts are single crystalline anatase TiO_2 (tetragonal a= 0.3785 nm, c=0.9415 nm). After the correction of the relative rotation between the image and the diffraction pattern, the growth direction of the nanobelt is determined to be [010]. This is supported by the high resolution TEM image in Fig.1(c), where the lattice fringes perpendicular to the growth direction has a spacing of 0.38 nm which is equal to the lattice parameter in the [010] direction. In addition, the crystallographic plane of two major exposed surfaces of the nanobelts is determined to be (101) facet as shown in Fig. 1(d), which is the most thermodynamically stable crystal facet of anatase TiO_2.[24] The details of the crystallographic plane identification can be seen in the Supporting Information.

The photocatalysis performance was evaluated in terms of the decomposition rate of methyl orange in an aqueous solution catalyzed by the TiO_2 nanoparticles under the ultraviolet (UV) A irradiation. Although the specific surface area of the nanospheres was about 2.8 times that of the nanobelts, the nanobelts exhibited better photocatalytic activity than the nanospheres (Figure 2). In order to clarify the underlying mechanism of the enhanced photocatalytic activity of the anatase TiO_2(101) nanobelts, we have investigated how the shape and the surface structure of the nanobelts affect the following four processes in photocatalysis: (a) light-irradiation induced formation of conduction-band electrons and valence band holes; (b) transfer of the photogenerated electrons and holes to the photocatalyst surface; (c) trapping of the photogenerated charge carriers at the photocatalyst surface and formation of reactive oxygen species (ROS); and (d) recombination of electron-hole pairs.

(a). Light absorption

Figure 3 shows the UV-visible spectra of the TiO_2 nanobelts and the nanospheres. Under the ultraviolet irradiation, electrons in the valence band absorb the photon energy and jump to the conduction band, leaving holes in the valence band. Light absorption is mainly determined by the band structure and the dipole matrix elements. It is deduced from Figure 3 that the bandgaps of the nanobelts and the nanospheres are almost identical (3.4 eV). Given their similar specific surface area, no evident difference in the light absorption efficiency was observed between the nanobelts and the nanospheres.

(b). Transfer of electrons and holes to the photocatalyst surface

Mobility of charge carriers in TiO_2 is one of the important factors that govern the photocatalysis efficiency. For example, although anatase TiO_2 has larger bandgap than rutile, it is more photoactive than rutile. One of the major reasons is that the electron mobility in anatase is 40 times greater than that in rutile.[25,26] Localized states lie within the mobility gap and their localization can impede the transfer of charge carriers to the reactive sites at the photocatalyst surface. To examine the mobility, the electronic density of states of the TiO_2 nanoparticles was calculated by FIREBALL. For a particular electronic state, the number of accessible atoms, W, describes the spatial extent of that state.[27] W gives a quantitative measure of the number of the atoms that a particular state reaches. The smaller the W, the more localized the state. Fig. 4 shows the states near the band edges of the nanobelts are less localized as compared to those in the nanospheres. In addition, localized states are absent in the bandgap of the nanobelts while present in the nanospheres. The ultraviolet light could excite the electrons from both the valence band and the localized midgap states to the conduction band, leaving the holes behind. These states in the midgap act as the traps for the photogenerated holes, and consequently act as the

recombination centers. As a result, these holes in the midgap will have very low mobility. In contrast, the holes in the valence band are expected to have larger mobility which can be transferred to the catalyst surface to directly oxidize the pre-adsorbed species.

In addition, the transport mobility of the charge carriers in the TiO_2 lattice was also calculated by the DFT method to quantitatively evaluate the capability of transporting charge carriers to the particle surface. Since the mobility is linearly related to the conductivity, one can estimate the conductivity, which is much easier to calculate. The natural approximate connection between the conductivity and the electronic states (localized states) and energies was considered to estimate the dc conductivity in the TiO_2 nanobelts and the nanospheres.[21,22] At room temperature the dc conductivity was estimated to be of the order of ~ 10^{-7} Ω^{-1} ·cm^{-1} for the nanobelts and ~ 10^{-9} Ω^{-1} ·cm^{-1} for the nanospheres. Our results give a crude estimation of the carrier transport in the nanostructures and show that the conductivity of the nanobelts is far greater than that of the nanospheres. Given that the conductivity is tied to the mobility, our results suggest that the carrier mobility in the nanobelts is much higher than that in the nanospheres.

(c). Trapping of charge carriers at the surface and formation of reactive oxygen species

Photogenerated charge carriers can react with electron donors or acceptors adsorbed on the surface of photocatalysts.[1–3, 28–30] Typically, for photocatalysts in an aqueous solution, the photogenerated valence-band holes interact with chemisorbed OH^- or H_2O to form surface-bound hydroxyl radical ($OH^\bullet$) and the conduction-band electrons react with adsorbed O_2 to form superoxide radical ($O_2^{\bullet -}$).[31–33] In the early studies, the hydroxyl radical[1,2] is considered as the main oxidative species responsible for the oxidation of organics although some reactions can also be initiated by direct hole oxidation especially when the adsorption of the substrate is extensive and the concentration of substrate is relatively high.[34] In recent studies, the superoxide radical has also been found to offer another reaction pathway for oxidative degradation of organics.[2,3,34–37] When TiO_2 is subject to light irradiation, electrons are excited from the valence band into the conduction band. It has been reported that adsorbed oxygen molecules act as the electron scavengers and combine with the electrons from the conduction band to form superoxide anions in air or in air-saturated water.[38–41] The concentration of superoxide increases with increase in the O_2 concentration. This indicates that during photocatalytic reactions photo-generated electrons are mainly trapped by adsorbed oxygen molecules, leading to the formation of superoxide.[40] The superoxide radical anion acts as an intermediate that can be involved in the oxidization of organics.[40,41]

In the present study, the amount of the photogenerated $OH^\bullet$ radical by the TiO_2 particles upon UV illumination in the aqueous solution was determined by the ESR signal intensity of the DMPO-$OH^\bullet$ adduct (Fig.5). ESR measurements gave direct evidence that the hydroxyl radicals were involved into the photocatalysis process. It was found that the nanobelts generated slightly less hydroxyl radicals than the nanospheres even though the nanobelts exhibited higher photocatalytic activity toward the decomposition of methyl orange. Therefore, it is deduced that decomposition of methyl orange was not solely via the oxidation of methyl orange by the hydroxyl radical.

Therefore, it is necessary to examine the role of superoxide radical in the photoctalysis. Superoxide radical has been reported to be formed via the adsorption of molecular O_2 on the TiO_2 surface in an aqueous solution and subsequent trapping of the photogenerated electrons.[42,43] Trapping of photogenerated electrons by molecular O_2 can affect the photocatalysis efficiency in two ways. In a direct way, the photoreduced superoxide radical anion acts as an intermediate that can be involved in the oxidization of organics.[40,41] In an indirect way, capture of the photogenerated electrons enables the accumulation of more reactive holes.[44,45] Even for a reaction photocatalyzed via the hydoroxyl radicals, it is coupled with reduction of

dissolved O_2 initially to peroxide and ultimately to water. The rate of hydroxyl radical- (or hole-) initiated oxidation cannot be faster than that of O_2 reduction by the photogenerated electrons. When O_2 is not reduced at a sufficiently high rate, the electrons accumulate on the photocatalyst and consequently increase the rate of radiationless electron-hole recombination. In this case, the rate of photooxidation is limited by the rate of O_2 reduction.[44,46,47] Hence the role of molecular O_2, a strong electron scavenger, in the photocatalysis process was examined. The decomposition reaction of methyl orange, which was photocatalyzed by the TiO_2 nanobelts and the nanospheres, proceeded in the aqueous solution under the ambient air, the O_2-saturated and the N_2-saturated conditions, respectively. For the decomposition reaction of methyl orange catalyzed by the nanobelts, the photocatalysis rate was enhanced when the aqueous solution was saturated with O_2 by bubbling oxygen gas into the solution while the photocatalysis rate was reduced under the N_2-saturated condition (Figure S3(a)). In contrast, switching from the O_2-rich to the O_2-deficient condition had little effect on the rate of the reaction photocatalyzed by the nanospheres (Figure S3(b)). These results suggest that adsorption and photoreduction of molecular O_2 on the TiO_2 nanobelt surface could be different from that on the nanosphere surface due to the difference in the shape and surface structure.

The adsorption and photoreduction of oxygen molecules on the nanobelt and nanosphere surfaces were further investigated using the FIREBALL simulation. For the anatase TiO_2 nanobelts, the two dominant surfaces are terminated by the (101) crystal plane. Therefore, it is reasonable to consider only the (101) facet in our calculations. The lattice parameters adopted in this calculation were compared with the the experimental result in Ref. [16], which has proved that FIREBALL is able to generate the correct lattice constants for anatase TiO_2 unit cell. The (101) facet was modeled using a slab by adding 20 Å of vacuum to a 384-atom bulk supercell containing eight TiO_2 layers. In this supercell, the geometry has been optimized by relaxing all the atomic positions without fixing any atoms on the bottom of the slab. Figure 6(a) shows the relaxed clean anatase TiO_2 (101) surface. The surface exposes fivefold (5*c*) and sixfold (6*c*) coordinated Ti atoms, as well as twofold (2*c*) and threefold (3*c*) coordinated O atoms. The calculated surface energy is 0.81 J/m^2, which is in good agreement with that calculated by Lazzeri *et al.* [24] The nanosphere is cut from a perfect bulk anatase supercell and put into a 100 Å vacuum box, with origin placed at the center of mass of the sphere. Some of the surface oxygen or titanium atoms are removed to ensure the electroneutrality. During the optimization the diameter of the nanosphere increases from 1.5 nm to 1.8 nm (Fig. 7(a)). The relaxed structure shows significant structural disorder on the surface of the nanosphere, with the presence of both undercoordinated Ti and O atoms. Besides the nanosphere with 144 atoms in this work, we have also carried out a series of calculations of anatase nanospheres with the size scale from 1.5 nm to 2.5 nm.[48] These calculations have showed that anatase nanopheres present significant structural disorders on the surfaces after optimization. The surface of the nanosphere shows the presence of fivefold (5*c*), fourfold (4*c*), and threefold (3*c*) coordinated Ti atoms, as well as threefold (3*c*) and twofold coordinated (2*c*) O atoms. It should be noted that the number of 5*c*-Ti sites is identical for the nanobelt (101) facet and the nanosphere. We estimate the strength of a molecule-surface interaction through the calculation of desorption enthalpies, ΔH_{des}.

Fig. 6(b) shows the optimized geometry of an O_2^- anion-molecule absorbed on a 5*c*-Ti site. The structure and geometry are in good agreement with that obtained by Mattioli *et al.* [43] In the O_2^- anion-molecule the two O atoms are both bonded to the 5*c*-Ti surface atom in a symmetric configuration with equal Ti-O distances, 2.02 Å, close to that in the bulk anatase. The formation of these two strong Ti-O bonds is confirmed by the value of the energy required to detach the ion-molecule from the surface, $\Delta H_{des} = -1.54$ eV. The absorbed O_2 molecule induces an acceptor electronic level in the energy gap, where the occupying electrons are mainly localized on the O_2 molecule. The presence of an acceptor close to the valence band

maximum (VBM) indicates that an electron transfer can easily occur from the surface to the molecule by forming an O_2^- radical, which is difficult to be detached from the surface.

For the nanosphere, one O_2^- ion-molecule was initially placed on the surface at a distance of 2.1 Å above one of the 5*c*-Ti sites of the nanosphere surface. During relaxation and molecular dynamics (MD) run, the molecule continuously changed its orientation, dissociated from the 5*c*-Ti sites, moved away from the surface and formed a weak bond with a 4*c*-Ti atom. This result is supported by the fact that the Ti-O distance between the Ti surface atom and one of the O atoms of the molecule was 2.70 Å while the Ti-O bond distance in the bulk was about 2.0 Å. In addition, the estimated energy to detach the O_2^- ion from the surface of the nanosphere was −0.53 eV. Next, two O_2^- anion-molecules were placed on the surface of the nanosphere. After geometry optimization, one of the molecules moved away from the surface to form a weak bond with a 4*c*-Ti atom, and the other did not dissociate from the 5*c*-Ti site. Instead there was a breaking of the bond between the weakly coordinated 3*c*-O and the 5*c*-Ti atoms involved in the adsorption (see Fig. 7(b)). The two oxygen atoms are both bonded symmetrically to the 4c-Ti atom with the Ti-O distances of 1.88 Å and 1.86 Å. These bonds are shorter than those in the bulk anatase. The O-O distance in the final configuration is 1.49 Å. These results are similar to that obtained by Mattioli *et al.* for the absorbed O_2^{-2} anion molecule on the anatase TiO_2 (101) surface.[43]

The above results show that the O_2 molecule-surface bonding is significantly strengthened by the capture of one electron on the anatase (101) facet of the TiO_2 nanobelt, whereas the O_2 molecule-surface bonding is weakened in the nanosphere. As a direct consequence, the single-crystalline nanobelts with the (101) facet has better capability of generating superoxide radical as compared to the nanospheres. As discussed above, promotion of the superoxide radical formation on the TiO_2 surface improves the photocatalysis efficiency. Since the (101) facet dominates the surface structure of the nanobelts, higher reactivity of oxygen molecules on the (101) facet is believed to be one of the origins of the enhanced photocatalytic activity of the nanobelts than the nanospheres.

(d). Recombination of electron-hole pairs

The photocatalysis efficiency is determined by the competition between the charge separation process and the charge recombination process, both in the bulk and surface. Photoluminescence (PL) spectra can be used to evaluate the charge recombination rate as reported in the previous studies,[49,50] because PL spectra directly arise from the radiative recombination processes of the electrons and the holes between two different energy states. Thereore, the PL spectra were obtained from the TiO_2 nanobelts and the nanospheres, respectively (Fig.S4 in Supporting Information). The peak centered at around 365 nm in the PL spectra was attributed to the emission of the band gap transition.[51] The peaks around 470 nm and around 550 nm were ascribed to the emissions from the charge transfer transition of oxygen vacancy trapped electrons.[49,52,53] The higher the PL emission intensity, the higher the recombination rate of the photogenerated electrons and holes. Figure S4 suggests that the nanobelts have a lower recombination rate than the nanospheres. The lower electron-hole recombination rate of the nanobelts originates from the following factors: (i) the charge carriers have higher mobility in the nanobelts than in the nanospheres; (ii) the single crystal nature along the longitudinal dimension of the nanobelts provides large space as the pathway for charge separation while the nanospheres are confined by the space; (iii) the anatase nanobelts with two dominant surfaces terminated by the (101) facet have higher reactivity with molecular O_2 than the nanospheres. More superoxide anions are formed by trapping the photogenerated electrons on the (101) faceted nanobelts. Thus more charge carriers are spatially separated on the nanobelt surface.

4. Conclusions

Although the TiO_2 nanobelts and the nanospheres possessed the same phase structure, similar specific surface area and photo-adsorption efficiency, the nanobelts exhibited better photocatalytic activity than the nanospheres. The nanobelts possessed higher charge carrier mobility and provided the pathway for transport of charge carriers throughout the longitudinal direction, which was expected to facilitate the charge separation. Our results indicate that the geometric shape of nanocrystal is an important factor in the catalyst design besides the specific surface area. Single-crystalline one-dimensional (nanobelts, nanowires and nanotubes) or two-dimensional (nanosheets) nanostructures are expected to show higher photocatalytic activity than zero-dimensional nanocrystal counterparts. The nanobelts showed an enhanced reactivity with O_2 molecules on the (101) facet, leading to more superoxide anions $(O_2^{\bullet -})$ on the photocatalyst surface. Generation of superoxide anions was a process of trapping the photogenerated electrons, which promoted the charge separation and resulted in a lower electron-hole recombination rate. Our work suggests that photocatalysis efficiency can be improved by tailoring the surface crystal structure.

Supplementary Material

Refer to Web version on PubMed Central for supplementary material.

Acknowledgments

This work was financially supported by a NSF grant (CBET-0834233), a NIH grant (1RC2ES018742-01), an ARTS grant from Eberly College of Arts and Sciences at West Virginia University and the Research Challenge Grant of West Virginia State (EPS08-01). The facilities and resources used in this work were partially supported by the NSF grant (EPS 0554328) with the matching funds from the West Virginia University Research Corporation and the West Virginia EPSCoR Office. The TEM experiments were carried out at Materials Characterization Center, LEXI/Calit2, University of California-Irvine. We are grateful to Dr. Dale Porter for facilitating the ESR measurement. N.W. conceived and designed the whole research, wrote the paper. J.W. synthesized the nanobelts, performed the photocatalysis experiment and wrote the data summary. D.T., J.L. and H.W. conducted the *FIREBALL* modeling. J.Z. was responsible for the TEM work. S.L. performed the ESR experiment. X.L. was involved into the data discussion and manuscript writing. A.M. participated in the data discussion.

References

1. Hoffmann MR, Martin ST, Choi W. Chem. Rev 1995;95:69.
2. Linsebigler AL, Lu GQ, Yates JT. Chem. Rev 1995;95:735.
3. Mills A, Le Hunte SJ. Photochem. Photobiol. A 1997;108:1.
4. Fujishima A, Zhang XT, Tryk DA. Surf. Sci. Rep 2008;63:515.
5. Grela MA, Colussi AJ. J. Phys. Chem 1996;100:18214.
6. Murakami N, Kurihara Y, Tsubota T, Ohno T. J. Phys. Chem. C 2009;113:3062.
7. Mor GK, Shankar K, Paulose M, Grimes CA. Nano Lett 2005;5:191. [PubMed: 15792438]
8. Gopal K, Mor GK, Shankar K, Paulose M, Varghese OK, Grimes CA. Nano Lett 2006;6:215. [PubMed: 16464037]
9. Mor GK, Varghese OK, Paulose M, Shankar K, Grimes CA. Solar Energy Mater. Solar Cells 2006;90:2011.
10. Machlin, ES. Materials Science in Microelectronics. New York: Elsevier; 2005. p. 26
11. Hotsenpiller PAM, Bolt JD, Farneth WE, Lowekamp JB, Rohrer GS. J. Phys. Chem. B 1998;102:3216.
12. Pang CL, Thornton G. Surf. Sci 2006;600:4405.
13. Taguchi T, Saito Y, Sarukawa K, Ohno T, Matsumura M. New J. Chem 2003;27:1304.
14. Ohno T, Sarukawa K, Matsumura M. New J. Chem 2002;26:1167.
15. Cho CH, Ho CH, Han MH, Kim DH, Kim DK. Mater. Chem. Phys 2005;92:104.

16. Yang HG, Sun CH, Qiao SZ, Zou J, Liu G, Smith SC, Cheng HM, Lu GQ. Nature 2008;453:638. [PubMed: 18509440]
17. Uchino T, Tokunaga H, Ando M, Utsumi H. Toxicology In Vitro 2002;16:629. [PubMed: 12206830]
18. Lewis JP, Glaesemann KR, Voth GA, Fritsch J, Demkov AA, Ortega J, Sankey OF. Phys. Rev. B 2001;64:195103.
19. Wang H, Lewis JP. J. Phys.: Condens. Matter 2006;18:421.
20. Tafen DN, Wang J, Wu NQ, Lewis JP. Appl. Phys. Lett 2009;94:093101.
21. Kubo R. J. Phys. Soc. Jpn 1957;12:570.
22. Greenwood DA. Proc. Phys. Soc 1958;71:585.
23. Abtew TA, Zhang M, Drabold DA. Phys. Rev. B 2007;76:045212.
24. Lazzeri M, Vittadini A, Selloni A. Phys. Rev. B 2001;63:155409.
25. Kera, Y.; Kominani, H.; Murakami, S. Photocatalysis: science and technology. In: Kaneko, M.; Okura, I., editors. Tokyo: Kodansha, Springer; 2002. p. 29-49.
26. Voinuv, M.; Augustynkim, J. Heterogeneous Photocatalysts. Schiavello, M., editor. New York: John Wiley and Sons; 1997. p. 1-42.
27. Lewis JP, Cheatham TE, Starikov EB, Wang H, Sankey OF. J. Phys. Chem. B 2003;107:2581.
28. Berger T, Sterrer M, Diwald O, Knzinger E, Panayotov D, Thompson TL, Yates JT. J. Phys. Chem. B 2005;109:6061. [PubMed: 16851666]
29. Henderson MA, Epling WS, Peden CHF, Perkins CL. J. Phys. Chem. B 2003;107:534.
30. Panayotov D, Yates JT Jr. Chem. Phys. Lett 2003;381:154.
31. Remillard JT, McBride JR, Nietering KE, Drews AR, Zhang X. J. Phys. Chem. B 2000;104:4440.
32. Ishibashi K, Fujishima A, Watanabe T, Hashimoto K. J. Phys. Chem. B 2000;104:4934.
33. Peiro AM, Colombo C, Doyle G, Nelson J, Mills A, Durrant JR. J. Phys. Chem. B 2006;110:23255. [PubMed: 17107174]
34. Kim S, Park H, Choi W. J. Phys. Chem. B 2004;108:6402. [PubMed: 18950128]
35. Schwitzgebel J, Ekerdt JG, Gerischer H, Heller A. J. Phys. Chem 1995;99:5633.
36. Cermenati L, Pichat P, Guillard C, Albini A. J. Phys. Chem. B 1997;101:2650.
37. Wang Y, Hong CS. Water Res 2000;34:2791.
38. Chatterjee D, Mahata A. Appl. Catal. B 2001;33:119.
39. Ishibashi K, Fujishima A, Watanabe T, Hashimoto K. J. Phys. Chem. B 2000;104:4934.
40. Kwon BG. J. Photochem. Photobiol. A 2008;199:112.
41. Fox MA, Chen CC. J. Am. Chem. Soc 1981;103:6757.
42. Nakamura R, Imanishi A, Murakoshi K, Nakato Y. J. Am. Chem. Soc 2003;125:7443. [PubMed: 12797819]
43. Mattioli G, Filippone F, Bonapasta AA. J. Am. Chem. Soc 2006;128:13772. [PubMed: 17044705]
44. Wang CM, Heller A, Gerischer H. J. Am. Chem. Soc 1992;114:5230.
45. Brezova V, Stasko A, Lapcik L Jr. J. Photochem. Photobiol. A 1991;59:115.
46. Berger T, Sterrer M, Diwald O, Knçzinger E. Chem. Phys. Chem 2005;6:2104. [PubMed: 16208752]
47. Henderson MA, White JM, Uetsuka H, Onishi H. J. Catal 2006;238:153.
48. Wang H, Lewis JP. J. Phys. Chem. C 2009;113:16631.
49. Li D, Haneda H, Hishita S, Ohashi N. Chem. Mater 2005;17:2596.
50. Cong Y, Zhang J, Chen F, Anpo M. J. Phys. Chem. C 2007;111:6976.
51. Li FB, Li XZ. Chemosphere 2002;48:1103. [PubMed: 12227516]
52. Lei Y, Zhang LD, Meng GW, Li GH, Zhang XY, Liang CH, Chen W, Wang SX. Appl. Phys. Lett 2001;78:1125.
53. Serpone N, Lawless D, Khairutdinov R. J. Phys. Chem 1995;99:16646.

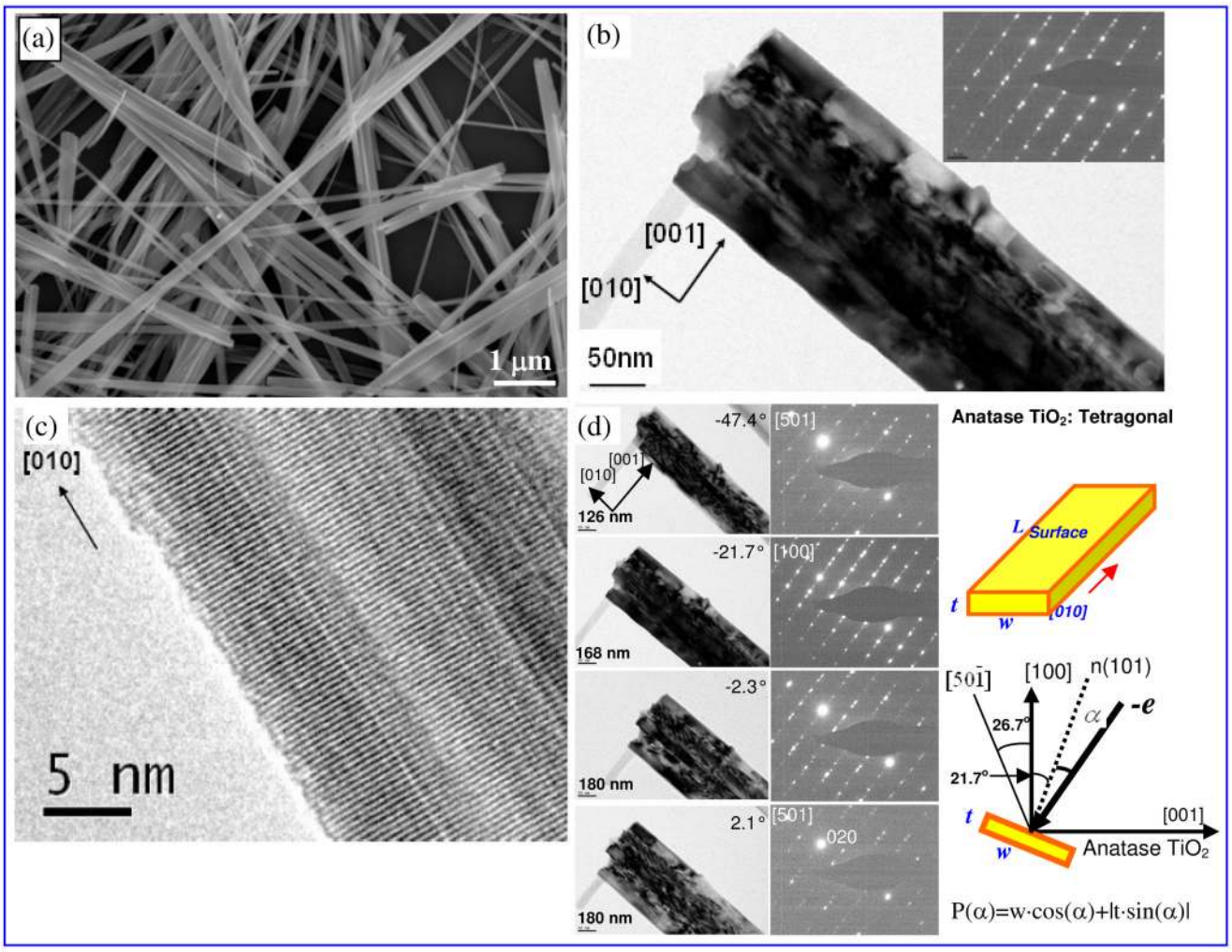

Figure 1.

(a) SEM images of the anatase TiO_2 nanobelts; (b) bright-field TEM image of a TiO_2 nanobelt, the inset is a selected area electron diffraction (SAED) pattern taken along the [100] direction of the nanobelt; (c) HRTEM image of a nanobelt; (d) bright-field TEM images and corresponding SAED patterns of a TiO_2 nanobelt recorded in different crystallographic orientations while keeping the [010] axis horizontal, as well as schematic illustrations of the nanobelt and the relationship between the incident beam and the nanobelt while taking images and diffraction patterns

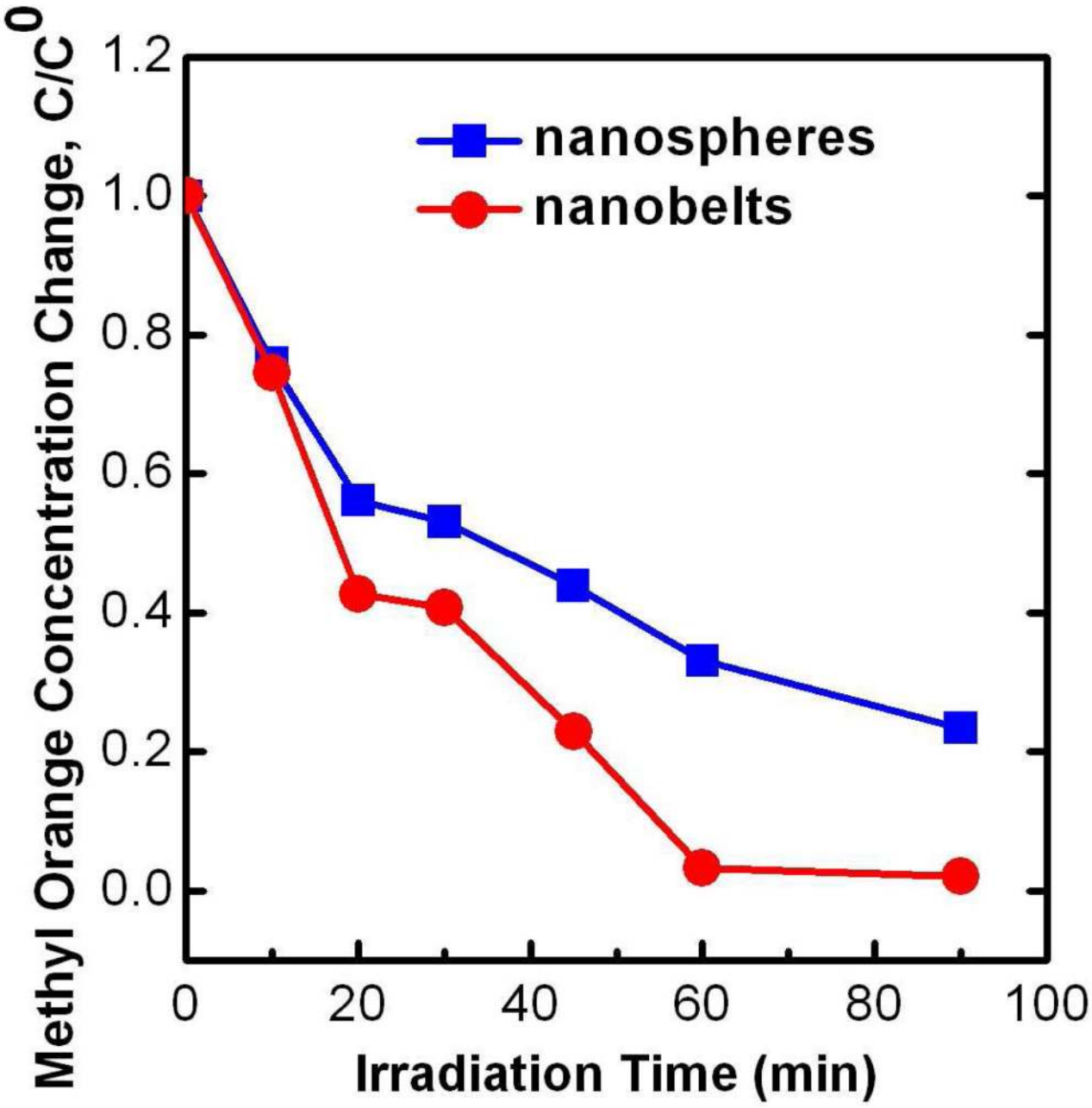

Figure 2.
Degradation of methyl orange in an aqueous solution by the TiO_2 nanobelts and the nanospheres as a function of exposure time to UV irradiation

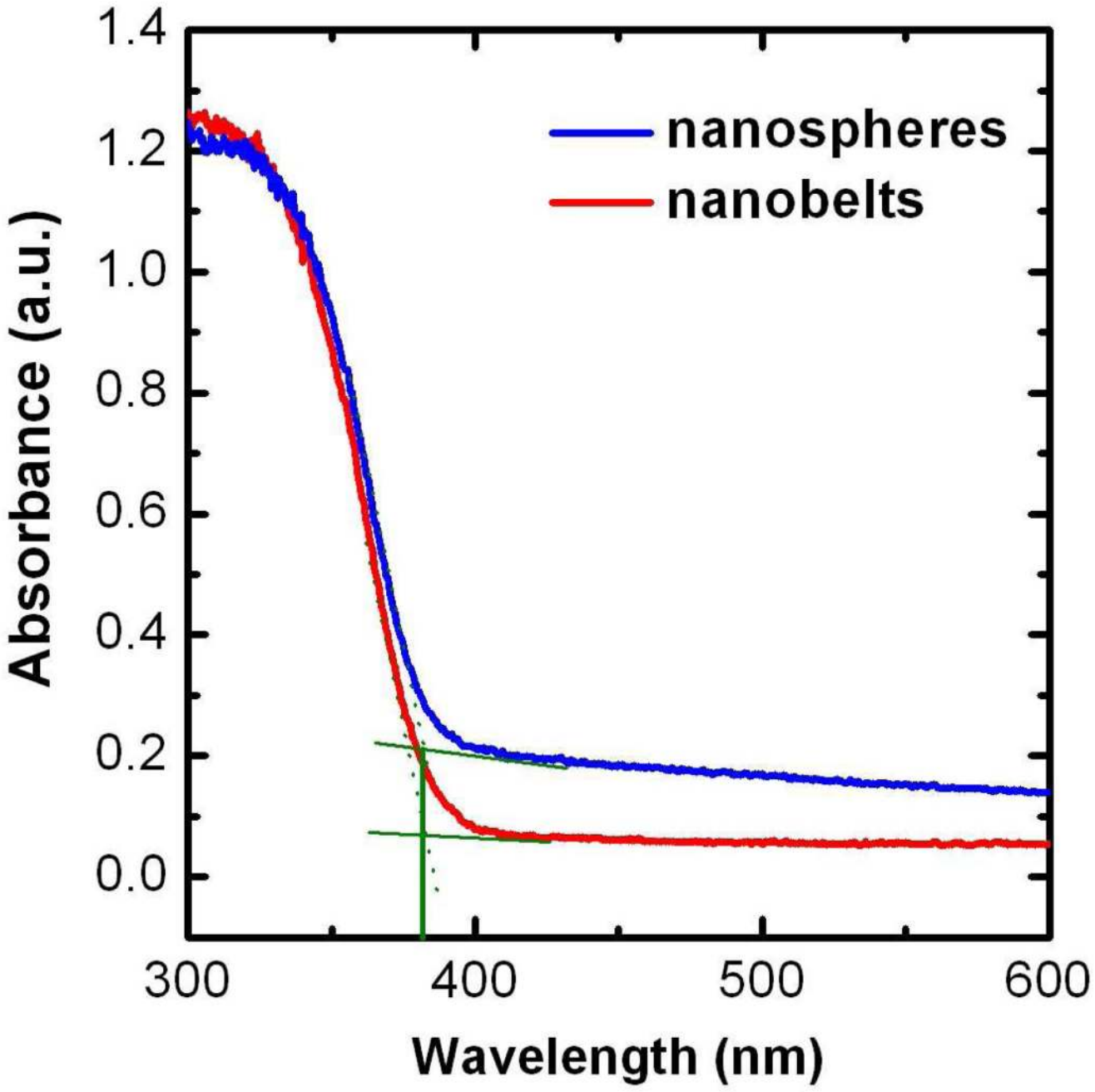

Figure 3.
Diffuse reflectance UV-visible spectra of the TiO_2 nanobelts and the nanospheres

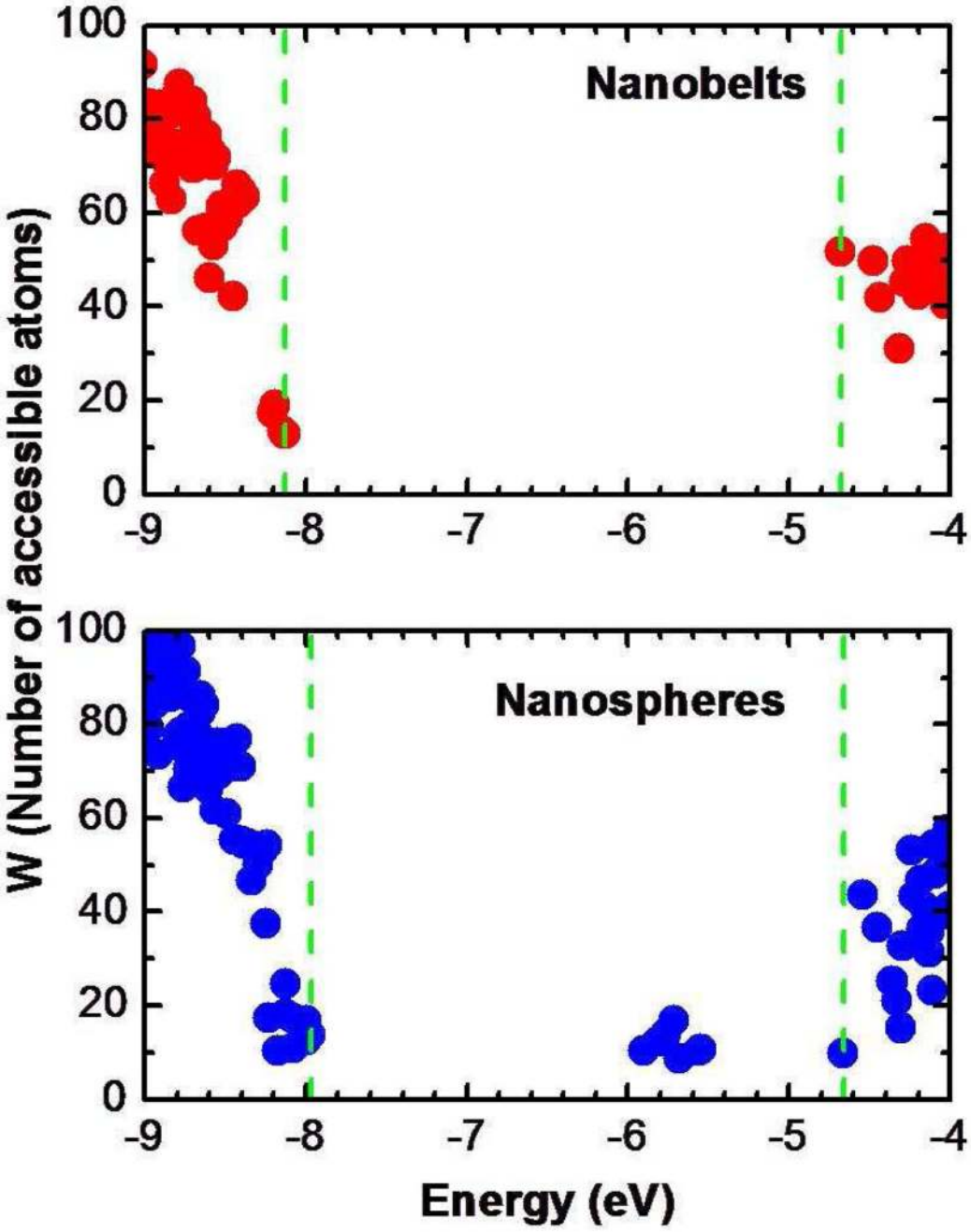

Figure 4.

Number of accessible atoms (*W*) for each electronic state near the valence and conduction band edges of the nanobelts and nanospheres. Note that the smaller *W*, the more localized the state. The dashed lines indicate the valence and conduction band edges

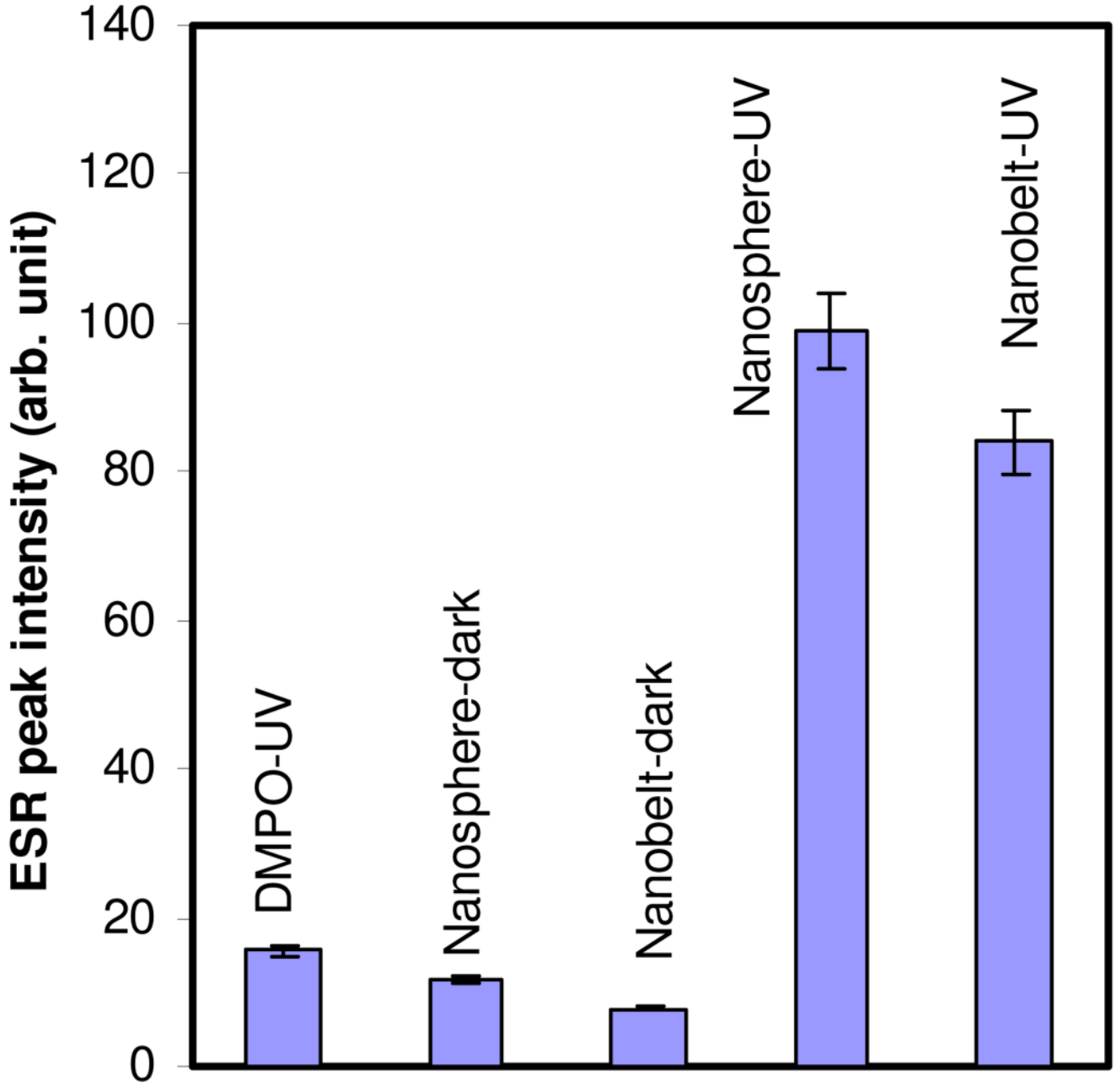

Figure 5.
The peak intensity of the ESR spectra obtained from the DMPO solution, the TiO_2 nanosphere-DMPO solution and the nanobelt-DMPO solution before and after UVA irradiation, indicating the amount of hydroxyl radical ($OH^{\bullet}$) photogenerated under different conditions

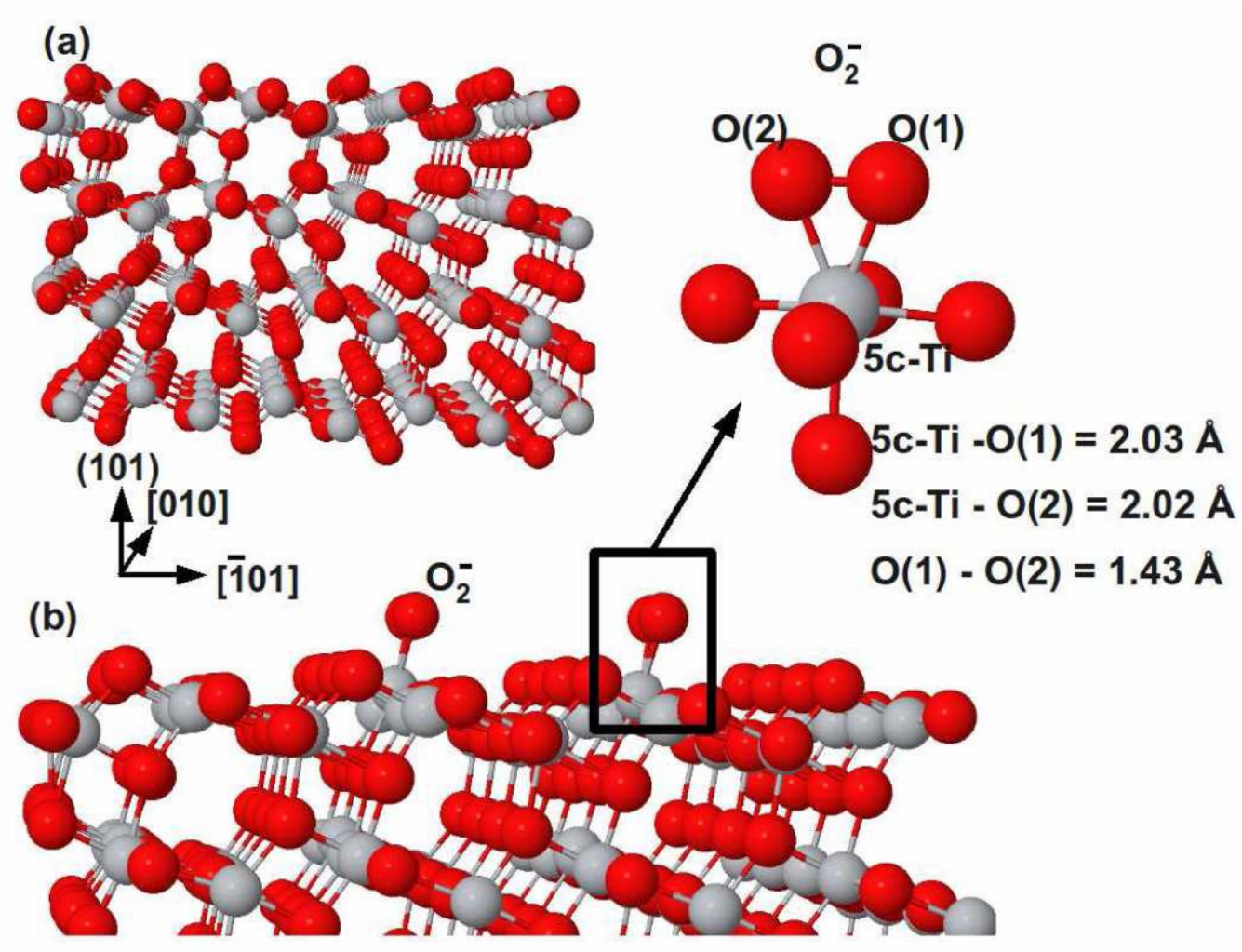

Figure 6.

Optimized geometries of (a) anatase (101) TiO_2 surface of the nanobelts; (b) O_2^- molecule absorbed at the five-fold coordinated Ti site on the surface. Note: Superoxide O_2^- is added from the beginning by adding an extra electron to the system.

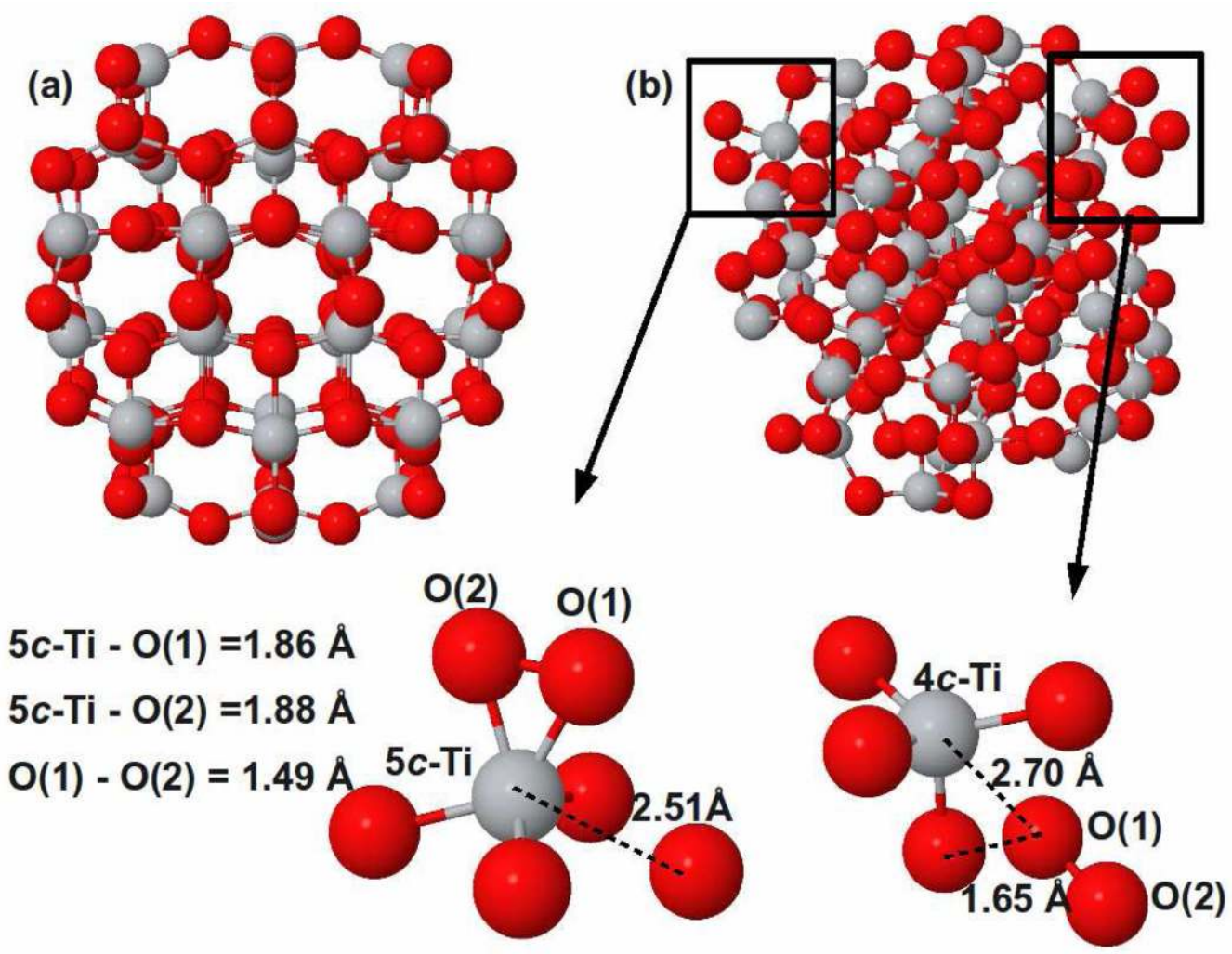

Figure 7.
Optimized geometries of (a) anatase TiO_2 nanosphere; (b) O_2^- molecule absorbed at the five-fold coordinated Ti site on a surface